Early Mars sub-aerial environments conducive to prebiotic evolution

William Rapin (✉ william.rapin@irap.omp.eu)

 Institut de Recherche en Astrophysique et Planétologie, Université de Toulouse 3 Paul Sabatier, CNRS, CNES

Gilles Dromart

 Universite de Lyon

Benton Clark

 Space Science Institute

Jürgen Schieber

 Indiana University

Edwin Kite

 University of Chicago   https://orcid.org/0000-0002-1426-1186

Linda Kah

 University of Tennessee   https://orcid.org/0000-0001-7172-2033

Lucy Thompson

 University of New Brunswick

Olivier Gasnault

 IRAP, Universite de Toulouse, CNRS, CNES   https://orcid.org/0000-0002-6979-9012

Jérémie Lasue

 IRAP   https://orcid.org/0000-0001-9082-4457

Pierre-Yves Meslin

 Institut de Recherche en Astrophysique et Planétologie (IRAP), Université Paul Sabatier-CNRS.
 https://orcid.org/0000-0002-0703-3951

Patrick Gasda

 Los Alamos National Laboratory

Nina Lanza

 Los Alamos National Laboratory   https://orcid.org/0000-0003-4445-7996

Physical Sciences - Article

Keywords:

Posted Date: November 22nd, 2022

Abstract

Mars provides a unique record for early habitable environments 1−3 but its potential for an independent origin of life is uncertain 4,5. Prebiotic chemical evolution leading to incipient life requires specific environments and processes to occur 6. In particular, wet-dry cycling is known to strongly promote the self-assembly of organics, generating opportunistic mixtures and combinations of essential biopolymers 7−9. However, evidence for such process has been missing from the geological record of Mars explored so far. Here we report on new observations by the Curiosity rover at Gale crater indicating wet-dry cycling occurred on early Mars. We observed exhumed centimetric polygonal ridges, with distinct Y-junctions, which are characteristic of a fossilized cracking pattern that initially formed in fresh mud by the sustained action of wet-dry cycles. Given organics are present in the ancient sediments of Gale, our results suggest the evaporitic basin has been particularly conducive to prebiotic polymerization processes. The features are physically and temporally associated with the transition from clay to sulfate-bearing strata, a key mineral assemblage found elsewhere across Mars. It suggests that the Noachian-Hesperian transition (3.8 − 3.6 Gyrs ago) as a whole has been favorable to prebiotic evolution.

Main Text

Mars has a well-preserved sedimentary record that date as far back as 4.3 Ga and perhaps earlier [10,11], and the early presence of habitable environments is now well-documented [1−3]. Early Mars had liquid water, energy sources, CHNOPS elements, catalytic transition metal elements, as well as B, Mg, Ca, Na and K, all of which are linked to existing and evolved life as we know it. Yet, much more uncertain is whether Mars' surface conditions were conducive to an independent origin of life [4,5], or abiogenesis, which is the natural process by which life may have arisen from initial non-living matter, such as simple organic compounds. Prebiotic chemistry leading to incipient life forms is thought to be restricted not only to certain limited conditions, but may even require a specific succession of distinct environmental changes for it to succeed [6]. As such, it differs substantially from more broadly defined requirements for habitability.

Here we report on new lithological and geochemical data from Hesperian-aged (~3.6 Gyrs old) strata of Mars that indicate wet-dry cycling, a process considered supportive of, and perhaps essential, for prebiotic chemical evolution [7−9]. *In situ* investigation of hundreds of meters of sedimentary stratigraphy within Gale crater has revealed a record of ancient aqueous surface environments from fluvio-lacustrine [12] to more intermittent lake or lake margin settings up-section. The latter is interpreted as seasonal or secular drying [13−15], or as discrete dry intervals [16]. After exploring strata dominated by clay-bearing mudstones, the rover reached the sulfate-bearing unit which is evidence for a major environmental transition [17] characteristic of stratified terrains found in other regions across Mars [18]. At this transition data collected by the rover uncovered a new type of sulfate-enriched evaporitic-clastic deposit.

Pervasive centimeter scale polygonal patterns in the basal sulfate-bearing stratigraphic unit manifest as straight ridges that intersect with triple junctions, with the most prominent occurrence observed on the 3154th mission sol (Fig. 1 and Extended Data Fig. 1). Several additional exhumed strata nearby show comparable, as well as incipient and altered variants of these patterns (Extended Data Fig. 3). The polygons persist to at least decimetric depth within the bedrock, as is evident from their stepped appearance on thick blocks of bedrock (Fig. 1b). On bedding planes these polygons are ~1 cm in height, and about 4 cm in diameter – varying between 1 and 7 cm (Extended Data Fig. 4). The ridges commonly consist of aligned nodules, variably juxtaposed, and irregular in shape and size (Fig. 1d). In contrast, polygons cores are smooth surfaced and represent the host bedrock. Chemical composition documented by the ChemCam instrument shows a significant increase of Ca-sulfate content and variable Mg-sulfate enrichment within the polygonal ridges and other nodular features, whereas the host bedrock is of basaltic bulk composition and sulfate-poor (Fig. 2 and Extended Data Table 2).

Although polygonal ridges commonly form in salt crusts and playas on Earth as a consequence of subsurface salinity convection [19], we do not favor this interpretation here. Terrestrial salt crusts are mostly pure and consist of ephemeral salt deposits that form larger polygons 0.5 to 2 m in size [20], and the lower gravity on Mars should have given rise to convection cells of even larger size than observed on Earth. Instead, we interpret the polygonal sulfate-bearing ridges as the fill of open desiccation cracks in muds by variably coalescent, salt-bearing and sediment-inclusive nodules (Fig. 3). Whereas desiccation cracks in fresh mud layers initially form T-junctions, maturation over repeated drying cycles results in convergence towards hexagonal shapes with junction angles near 120°, i.e. Y-junctions [21]. In experiments, using multi-millimetric clay layers, joint angles tend towards 120° after 10 consecutive dryings with significantly more cycles required to mature pattern into hexagonal shapes [22].

The abundance of 30 to 50 wt.% Ca-sulfate and up to 40 wt.% Mg-sulfate measured within the ridges and nodular bedrock and their much lower abundance in the host bedrock (Fig. 2) collectively suggest that sulfate minerals precipitated with evaporation in muds and incorporated detrital sediment in the process. The present appearance of the sulfate-bearing ridges likely is not the original configuration of these features. Rather they started out as evapoconcentration focused on initially formed cracks that then evolved over a longer history of drying cycles and burial diagenesis (Fig. 3). They are now exposed as erosion resistant polygonal ridges due to their higher degree of cementation relative to the host bedrock, and an early bias of surface salt precipitation in original mud-crack polygons (Fig. 3d).

Recurrent wetting of surface muds likely reflects a combination of flooding and groundwater recharge. Flooding could have dissolved salts that formed ephemeral surface crusts, as well as adding sediment and promoting burial, although air-fall is another possible source for sediment addition. The polygons' size range of a few centimeters (Fig. 1), suggests that desiccation and mud contraction affected only the uppermost few centimeters of the surface muds [22]. The variability in shape and size of the sulfate-rich nodules that precipitated within the ridges indicates several generations of nodule growth, in consistence with significant intra-sediment salinity fluctuations due to repeated drying cycles (Fig. 3).

Given the apparent repetition and limited desiccation depth, the associated wet-dry cycles could have been seasonal but potentially also active on shorter time scales. The time span during which these wet-dry cycles left their intermittent signature in the sediments may be approximated via the thickness of the polygon-bearing stratigraphic interval (18 m). Using terrestrial analogs for sedimentation rate [23], thousands to millions of years may be indicated. Even under assumption of the shorter estimate, the duration over which wet-dry cycling in evaporative ponds may have recurred in Gale crater is significant relative to the timescale considered favorable to prebiotic chemical evolution [24].

The two major observations on polygonal features combine the hexagonal shapes that indicates repeated drying cycles, and their persistence within stratigraphic thickness implying wet-dry conditions were maintained in the long-term. Mud cracks were observed in underlying strata of the Murray formation, but predominantly formed T-junctions that suggest a single desiccation event [14,16].

The polygonal features described here are the first tangible evidence for sustained wet-dry cycling on early Mars, a process considered strongly supportive for prebiotic chemical evolution. During dryings, water activity is lowered and the concentration of soluble ingredients in the residual liquid is increased, boosting reaction rates, especially for higher-order reactions [7]. For instance, the reactions that form nucleotides from their constituent nucleobases (ribose, phosphate) produce H_2O and hence are favored at low water activity. Most importantly, the polymerization reactions necessary to advance from nucleotides to RNA or DNA, and from amino acids to proteins, require dehydration steps which have been demonstrated to be facilitated by wet–dry cycles [25–27]. Under the right environmental conditions Darwin's proverbial "warm little pond" could significantly promote the reactions for macromolecule polymerization, and through sustained wet-dry cycling increase the likelihood of chemical evolution towards the origination of life [24].

In a broader regional context, there is widespread documentation of preserved organics in ancient Gale crater strata, containing up to ~0.5 kg/m^3 [3,28], in addition to a variety of other soluble elements [3]. The addition of direct evidence for a series of repeated wet-dry cycles presented here supports that conditions in ancient Gale crater were conducive to prebiotic polymerization processes. There is definite potential for wet-dry cycling to have occurred more broadly on Mars (Fig. 4) in the period when both intrabasin sulfate salts and clays were deposited [1] as Gale is a stratigraphy of global significance for this mineral assemblage near the Noachian-Hesperian transition [29]. Some of these strata may thus harbor well-preserved evidence of prebiotic chemical evolution, a record that is no more available on Earth [30]. On the basis of this new evidence for sub-aerial wet-dry cycling within early habitable environments, and considering the delivery of organics and accumulation of volatiles on the Martian surface for almost a billion years prior (Fig. 4), our findings suggest that the Noachian-Hesperian transition period could have been favorable for the emergence of life; possibly more than the earlier Noachian eon that has potential for perennially wet surface environments [18].

Methods

Rover-based geochemical datasets and data processing. The Curiosity rover has 5 instruments that can measure geochemistry and mineralogy [34]. Thus, ChemCam is the primary source of available chemical data. ChemCam is a laser-induced breakdown spectrometer (LIBS) that provides chemical analyses at a submillimeter scale and detailed images with the Remote Micro Imager (RMI) [35,36]. Major-element contents were obtained using the current calibration model [37]. Water and sulfate contents were estimated using dedicated calibration models : for water content quantification uses the hydrogen signal [38], and for sulfate content the sulfur signal is used with in situ calibration as previously described for sulfate enrichments observed elsewhere in the Murray formation [14]. Although the arm-mounted APXS instrument did not sample polygonal ridges owing to operational constraints, it provided a bulk (~2 cm diameter area) measurement on brushed, smoothed host bedrock immediately adjacent to a raised, resistant ridge (Fig. 1c) highlighting the absence of sulfate enrichment (Extended Data Table 2). APXS data from other bedrock targets and resistant features in the vicinity of the polygonal features also support the concentration of Mg- and Ca-sulfates in the resistant features (Extended Data Fig. 6). CheMin and SAM analyses (which provide mineralogy and evolved gas analysis respectively from powdered, drilled sample) were not acquired on the polygonal ridges and most of the nodular bedrock.

Identification of the nodular lithology. The nodular lithology was identified based on images using both MastCam and ChemCam RMI. The lithology is characterized by protruding, erosion-resistant forms of near centimeter-scale connected to the host bedrock. They are variably shaped, widespread and abundant in the examined section (Extended Data Fig. 3). The ChemCam RMI was used to associate point by point the LIBS measurements with either smooth host bedrock (e.g. Extended Data Fig. 7) or nodular bedrock (e.g. Extended Data Fig. 8). This careful classification of all ChemCam data acquired within the examined section provides exhaustive geochemical data from the bedrock, removing points with soil contribution or bad laser focus. The full list of points classified from either host or nodular is shown on Extended Data Table 3.

Lithology of sulfate-bearing nodular bedrock. Nodules are widespread, highly variable in density in the examined section (Extended Data Fig 3), and occur as three morphologic types: rounded, dendritic, and vacuolar. Rounded forms are up to 1 cm in diameter and more resistant to erosion than the host bedrock. Nodules can be spherical to sub-spherical, and can show variable clustering and coalescence to form incipient to well-developed nodular ridges (Extended Data Fig. 9a,b). Dendritic nodules are jagged, multifaceted, multi-centimeter forms that are evenly distributed on bedding planes at certain intervals, and resemble rosette-like aggregates (Extended Data Fig. 7meda,b,d). The vacuolar nodules are large (up to decimeter scale), polymorphic forms which apparently resulted from random amalgamation of nodules. Their coalescence is partial. Now visible voids likely represent spots once occupied by uncemented host bedrock that has been removed by eolian erosion processes [39]. Vacuolar nodules are pervasive at the top of the studied interval (Extended Data Fig. 11). Outcrops with laminae consisting of variably coalescent micro-nodules were also observed within the section, although not analyzed by the rover chemical instruments (Extended Data Fig. 9e).

Polygonal Pattern Size Analysis. To generate the map over which the polygonal pattern was analyzed (Extended Data Fig. 4a), we used the Onsight software (https://software.nasa.gov/software/NPO-50830-1) which was developed by the Jet Propulsion Laboratory for the context of Mars exploration. Onsight renders a three-dimensional reconstruction and visualization of the surface of Mars from a variety of images. For our purpose, it allowed orthoprojection to the surface, with orthoprojected scale, of the Mastcam mosaics.

Most of the polygon morphologies are hexagonal, and resemble honeycomb or hexagon floor tiles. Pentagonal forms are common. Rare quadrangle and heptagonal patterns have also been observed. The size of the polygons is approximated by the diameter of the circles that are enclosed within the polygons, i.e. circles that are tangential to polygon sides. The circles were manually drawn, and diameter of the individual polygons was measured using Adobe Illustrator® software applied to the Onsight orthoprojection of the mosaics acquired on sols 3152 - 3154 (West Section) (Extended Data Fig. 4a). The polygons that were selected for analysis are those that offer a fairly regular shape, i.e. the polygons that have equal to subequal side lengths. The unmarked areas are those for which late diagenetic veins intersect and disturb the original polygonal ridge pattern, and those for which the original polygonal ridges have been stripped off after exhumation by dissolution and/or deflation.

The average diameter of the 467 circles that were analyzed by a single operator over a surface of about 3.75 square meters is 3.9 cm, with the smallest and largest specimen at 1.73 cm and 7.56 cm, respectively (Extended Data Table 1). To have a notion of the degree of precision of our method, a second operator made a test by repeating the marking and measurements over Block 1 (Extended Data Fig. 4a). The test revealed that: (i) the number of polygons distinguished by the operators is minimal, i.e. 168 against 176; (ii) mean size varies from 3.43 to 3.98 cm, which is a relative error of only ~16%, at best.

The frequency distribution of diameter cm values shows an unimodal asymmetrical, i.e. Poisson probability distribution (Extended Data Fig. 4b). Distinct blocks of similar areas yield similar polygonal pattern's characteristics (Extended Data Table 1), which suggests the polygon-bearing bedrock originally was homogeneous in terms of texture (porosity; grain-size) and mineralogical composition, laterally at multi-metric scale.

Declarations

Author contributions:

W.R. and G.D. equally led the writing of the manuscript. W.R., G.D., B.C.C., J.S., L.C.K., L.M.T., P.J.G., P.Y.M. and J.L. contributed to methodology, investigation and data processing. O.G. and N.L.L. are the leads of the ChemCam instrument investigation. J.S. and E.S.K. provided significant contributions to the writing and reviewing of the manuscript. All co-authors provided helpful comments and inputs to the manuscript.

References

1. Ehlmann, B. L. & Edwards, C. S. Mineralogy of the Martian Surface. *Annu. Rev. Earth Planet. Sci.* **42**, 291–315 (2014).
2. Wordsworth, R. The Climate of Early Mars. *Annu. Rev. Earth Planet. Sci.* **44**, 381–408 (2016).
3. Vasavada, A. R. Mission Overview and Scientific Contributions from the Mars Science Laboratory Curiosity Rover After Eight Years of Surface Operations. *Space Sci. Rev.* **218**, 1–65 (2022).
4. Clark, B. C. *et al.* Origin of Life on Mars: Suitability and Opportunities. *Life* **11**, 539 (2021).
5. Mojarro, A., Jin, L., Szostak, J. W., Head III, J. W. & Zuber, M. T. In search of the RNA world on Mars. *Geobiology* **19**, 307–321 (2021).
6. Sasselov, D. D., Grotzinger, J. P. & Sutherland, J. D. The origin of life as a planetary phenomenon. *Sci. Adv.* **6**, eaax3419 (2020).
7. Campbell, T. D. *et al.* Prebiotic condensation through wet–dry cycling regulated by deliquescence. *Nat. Commun.* **10**, 4508 (2019).
8. Becker, S. *et al.* Wet-dry cycles enable the parallel origin of canonical and non-canonical nucleosides by continuous synthesis. *Nat. Commun.* **9**, 163 (2018).
9. Damer, B. & Deamer, D. The Hot Spring Hypothesis for an Origin of Life. *Astrobiology* **20**, 429–452 (2020).
10. Farley, K. A. *et al.* In Situ Radiometric and Exposure Age Dating of the Martian Surface. *Science* **343**, 1247166 (2014).
11. Goodwin, A., Garwood, R. J. & Tartèse, R. A Review of the "Black Beauty" Martian Regolith Breccia and Its Martian Habitability Record. *Astrobiology* **22**, 755–767 (2022).
12. Grotzinger, J. P. *et al.* Deposition, exhumation, and paleoclimate of an ancient lake deposit, Gale crater, Mars. *Science* **350**, aac7575 (2015).

13. Hurowitz, J. A. *et al.* Redox stratification of an ancient lake in Gale crater, Mars. *Science* **356**, eaah6849 (2017).

14. Rapin, W. *et al.* An interval of high salinity in ancient Gale crater lake on Mars. *Nat. Geosci.* **12**, 889–895 (2019).

15. Schieber, J. *et al.* Mars is a mirror – Understanding the Pahrump Hills mudstones from a perspective of Earth analogues. *Sedimentology* **69**, 2371–2435 (2022).

16. Stein, N. *et al.* Desiccation cracks provide evidence of lake drying on Mars, Sutton Island member, Murray formation, Gale Crater. *Geology* **46**, 515–518 (2018).

17. Milliken, R. E., Grotzinger, J. P. & Thomson, B. J. Paleoclimate of Mars as captured by the stratigraphic record in Gale Crater. *Geophys. Res. Lett.* **37**, L04201 (2010).

18. Bibring, J.-P. *et al.* Global Mineralogical and Aqueous Mars History Derived from OMEGA/Mars Express Data. *Science* **312**, 400–404 (2006).

19. Lasser, J., Nield, J. M. & Goehring, L. Surface and subsurface characterisation of salt pans expressing polygonal patterns. *Earth Syst. Sci. Data* **12**, 2881–2898 (2020).

20. Goodall, T. M., North, C. P. & Glennie, K. W. Surface and subsurface sedimentary structures produced by salt crusts. *Sedimentology* **47**, 99–118 (2000).

21. Goehring, L., Conroy, R., Akhter, A., J. Clegg, W. & F. Routh, A. Evolution of mud-crack patterns during repeated drying cycles. *Soft Matter* **6**, 3562–3567 (2010).

22. Goehring, L. Evolving fracture patterns: columnar joints, mud cracks and polygonal terrain. *Philos. Trans. R. Soc. Math. Phys. Eng. Sci.* **371**, 20120353 (2013).

23. Sadler, P. M. Sediment Accumulation Rates and the Completeness of Stratigraphic Sections. *J. Geol.* **89**, 569–584 (1981).

24. Clark, B. C. & Kolb, V. M. Macrobiont: Cradle for the Origin of Life and Creation of a Biosphere. *Life* **10**, 278 (2020).

25. Becker, S. *et al.* Unified prebiotically plausible synthesis of pyrimidine and purine RNA ribonucleotides. *Science* **366**, 76–82 (2019).

26. Higgs, P. G. The Effect of Limited Diffusion and Wet-Dry Cycling on Reversible Polymerization Reactions: Implications for Prebiotic Synthesis of Nucleic Acids. *Life* **6**, E24 (2016).

27. Ross, D. S. & Deamer, D. Dry/Wet Cycling and the Thermodynamics and Kinetics of Prebiotic Polymer Synthesis. *Life* **6**, 28 (2016).

28. Stern, J. C. *et al.* Organic carbon concentrations in 3.5-billion-year-old lacustrine mudstones of Mars. *Proc. Natl. Acad. Sci.* **119**, e2201139119 (2022).

29. *Sedimentary Geology of Mars*. (SEPM, 2012). doi:10.2110/pec.12.102.

30. Knoll, A. H. Paleobiological Perspectives on Early Microbial Evolution. *Cold Spring Harb. Perspect. Biol.* **7**, a018093 (2015).

31. Thomson, B. J. *et al.* Constraints on the origin and evolution of the layered mound in Gale Crater, Mars using Mars Reconnaissance Orbiter data. *Icarus* **214**, 413–432 (2011).

32. Le Deit, L. *et al.* Sequence of infilling events in Gale Crater, Mars: Results from morphology, stratigraphy, and mineralogy. *J. Geophys. Res. Planets* **118**, 2439–2473 (2013).

33. Kite, E. S. Geologic Constraints on Early Mars Climate. *Space Sci. Rev.* **215**, 10 (2019).

Methods references:

34. Grotzinger, J. P. *et al.* Mars Science Laboratory Mission and Science Investigation. *Space Sci. Rev.* **170**, 5–56 (2012).

35. Maurice, S. *et al.* The ChemCam Instrument Suite on the Mars Science Laboratory (MSL) Rover: Science Objectives and Mast Unit Description. *Space Sci. Rev.* **170**, 95–166 (2012).

36. Wiens, R. C. *et al.* The ChemCam Instrument Suite on the Mars Science Laboratory (MSL) Rover: Body Unit and Combined System Tests. *Space Sci. Rev.* **170**, 167–227 (2012).

37. Clegg, S. M. *et al.* Recalibration of the Mars Science Laboratory ChemCam instrument with an expanded geochemical database. *Spectrochim. Acta Part B At. Spectrosc.* **129**, 64–85 (2017).

38. Rapin, W. *et al.* Quantification of water content by laser induced breakdown spectroscopy on Mars. *Spectrochim. Acta Part B At. Spectrosc.* **130**, 82–100 (2017).

39. Schieber, J. *et al.* Engraved on the rocks—Aeolian abrasion of Martian mudstone exposures and their relationship to modern wind patterns in Gale Crater, Mars. *Depositional Rec.* **6**, 625–647 (2020).

40. Hartmann, W. K. & Neukum, G. Cratering Chronology and the Evolution of Mars. *Space Sci. Rev.* **96**, 165–194 (2001).

41. Quantin-Nataf, C., Craddock, R. A., Dubuffet, F., Lozac'h, L. & Martinot, M. Decline of crater obliteration rates during early martian history. *Icarus* **317**, 427–433 (2019).
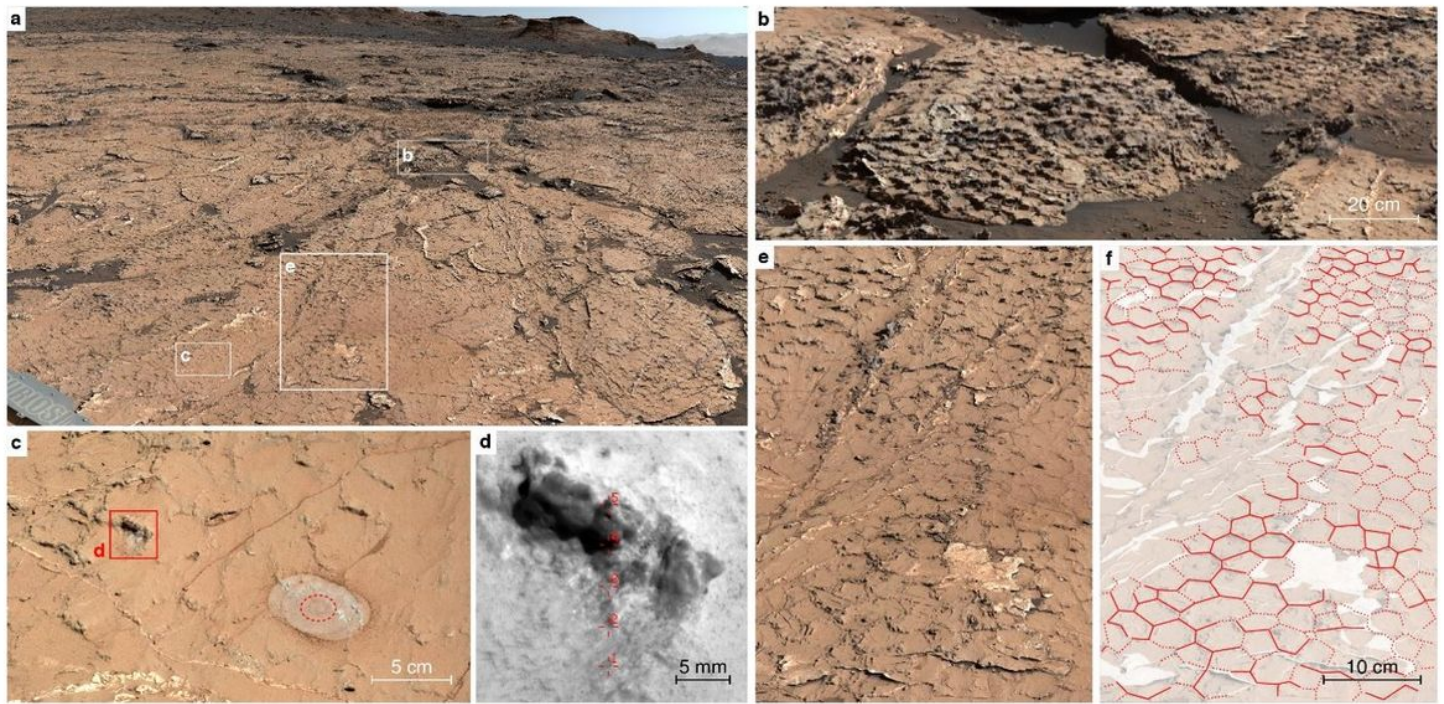
Figures

Figure 1

Polygonal ridges - *in situ* observations. **a**, General view of bedrock surrounding the rover on sols 3154 to 3156 showing widespread polygonal ridges (mcam00270; larger image Extended Data Fig. 2). **b**, Close-up showing "stepped" exposure of polygons within large bedrock blocks. **c**, View of bedrock (mcam00287) with polygons and locations of ChemCam analysis (red rectangle) and APXS analysis with approximate footprint (dotted circle). **d**, Remote micro-image of cemented ridge with spots analyzed by ChemCam (reticles 1 to 5), highlighting details of nodular texture (ccam01156). **e**, Bedrock with polygonal pattern and interpretative overlay (**f**) that shows prominent ridges (solid red lines), less certain ridges (dotted red lines), and crosscutting later stage Ca-sulfate filled veins (white areas) (mcam00276).
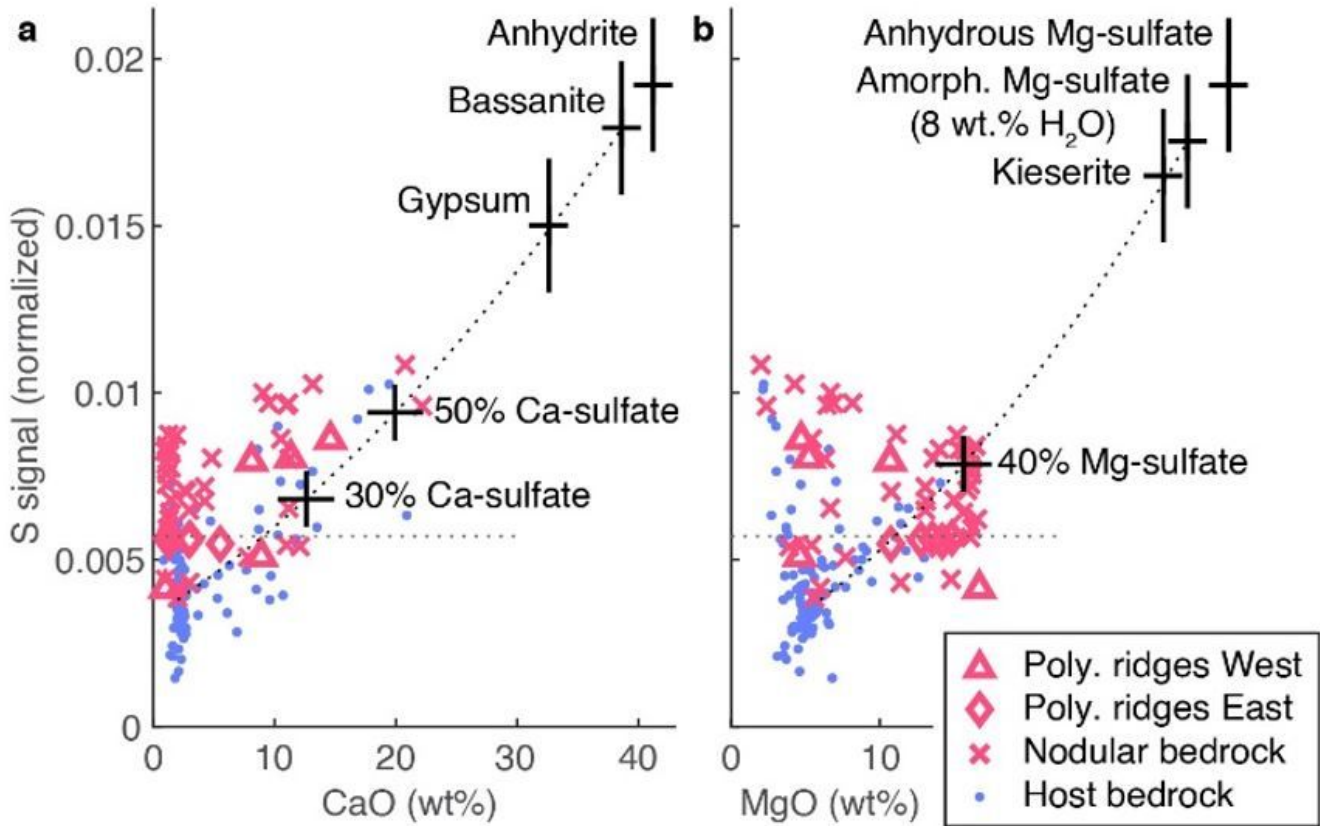
Figure 2

Bedrock enrichments in Ca/Mg-sulfate. ChemCam sulfur signal as a function of CaO (**a**) and MgO (**b**) for smooth host bedrock (blue) and nodular bedrock (red). Dotted line corresponds to mixing of sulfates with average siliciclastic host bedrock ; end-members are shown by black crosses. The sulfur signal limit of detection at $SO_3 > 10.6$ wt.% is also shown (horizontal dashed line). Vertical error bars on end-members represent sulfate content calibration uncertainty.

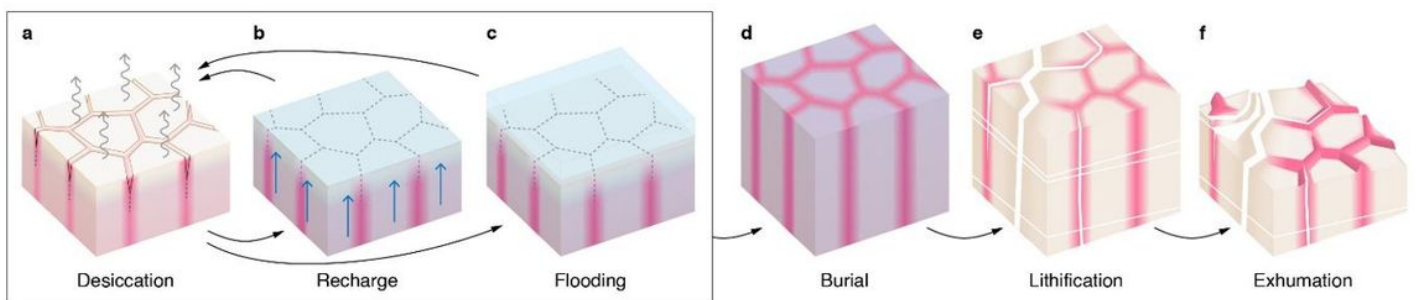**Figure 3**

Formation model for sulfate-enriched polygonal ridges. Repeated cycles of desiccation (**a**), recharge (**b**) and flooding (**b**) form a vertically propagating hexagonal pattern of sulfate enrichment. **a**, Evaporation desiccates and cracks near-surface sediment, triggering salt crystallization (red) at and near cracks where the subsurface brine (purple) concentrates. **b**, Water recharge heals cracks by sediment hydration. **c**, Flooding dissolves excess salts at the surface but subsurface brine and intrasediment sulfate salts are preserved and siliciclastic sediment is deposited on top. **d**, Sediment is buried with saturated brine in pore spaces and sulfates are mostly preserved. **e**, Later diagenesis partially dissolves intra-sediment sulfate salts and late diagenetic fractures are filled with Ca-sulfate (white). **f**, Sulfate-cemented polygonal ridges become visible during exhumation as the softer host bedrock is preferentially removed during weathering.
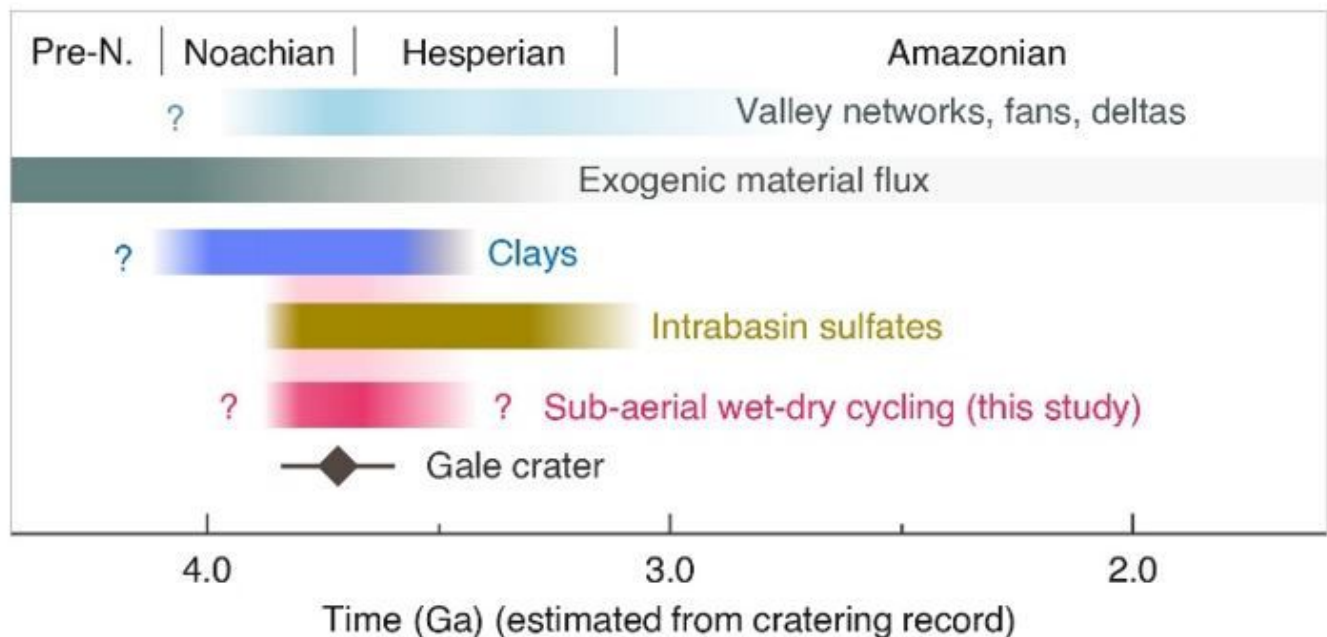

Figure 4

Mars' potential for prebiotic record. Evidence for sub-aerial wet-dry cycling could be relevant to the early Noachian-Hesperian transition period during which both intrabasin sulfates and clays formed [1]. Timing for Gale impact (diamond) with uncertainty covers the different reported ages [31,32]. Exogenic material flux is a proxy for the delivery of organics to the surface (Extended Data Fig. 5). Timing for valley networks, fans and deltas reported by crater counting on geomorphic features [33].

Supplementary Files

This is a list of supplementary files associated with this preprint. Click to download.

- wrapinevappolygonssupplementary.docx